Earth and Planetary Science Letters 380 (2013) 12–20

Contents lists available at ScienceDirect

Earth and Planetary Science Letters

www.elsevier.com/locate/epsl

Global patterns and vigor of ventilated hydrothermal circulation through young seafloor

D. Hasterok [1]

Institute for Geophysics and Planetary Physics, Scripps Institution of Oceanography, 9500 Gilman Dr. MS 0225, La Jolla, CA 92093-0225, USA

ARTICLE INFO

Article history:
Received 9 April 2013
Received in revised form 25 June 2013
Accepted 7 August 2013
Available online 4 September 2013
Editor: C. Sotin

Keywords:
heat flow
heat flux
hydrothermal circulation
oceanic heat loss
sedimentation

ABSTRACT

Using an updated global heat flow dataset with >14 000 oceanic measurements, we revise the estimated global power deficit due to ventilated hydrothermal circulation. This study differs from previous estimates by taking into account (1) non-Gaussian statistics, (2) an improved seafloor age model, (3) a new plate cooling model calibrated directly to heat flow, and (4) the effect of sediment cover on the heat flow deficit and ventilated cutoff age. We obtain the maximum heat flow deficit (difference between predicted and observed) when the data are separated by seafloor areas with <400 m and ⩾400 m of sediment cover. The estimated power deficit (integrated heat flow deficit with respect to area) for areas of thin (<400 m) sediment cover is 7.8 TW and for areas of thick (⩾400 m) is 0.2 TW. The total power deficit, 8.0 TW with 50% of estimates falling between 5.0 and 10.0 TW, represents a ~30% reduction in magnitude compared with previous heat flow and fluid flow based estimates. Regions with thick, ⩾400 m, sediment cover experience half the heat flow deficit for one-third of the duration (25 Ma) of regions with thin sediment cover (75 Ma). Based on this study, vigorous fluid exchange between the oceans and seafloor redistributes ~30% of heat lost through young oceanic crust.

1. Introduction

The observation of pervasive hydrothermal circulation through the seafloor (Lister, 1972) was rapidly accepted as the cause for an observational heat flow deficit relative to conductive cooling models of the oceanic lithosphere (Williams and Von Herzen, 1974; Sclater et al., 1980; Stein and Stein, 1994). This observational deficit is largest near the mid-ocean ridge axis and gradually decreases in magnitude until the heat flow is consistent with conductive cooling estimates at ~75 Ma (Fig. 1A and B). Extensive sediment cover inhibits flow between the ocean and crust, eventually choking off ventilated flow as all igneous outcrops are blanketed (Davis and Elderfield, 2004). This sedimentation effect has long been recognized (Lister, 1972; Anderson and Hobart, 1976; Davis and Lister, 1977; Sclater et al., 1976; Sclater et al., 1980), but has not been incorporated into calculations of the global power deficit.

Previous heat flow based studies (Sclater et al., 1980; Stein and Stein, 1994) used all available heat flow observations and assumed the entire seafloor area within any given age bin contributes to the power deficit. While there is good evidence for hydrothermal circulation within the igneous crust of old >80 Ma seafloor and beneath thick sediment cover (Fisher and Von Herzen, 2005), it contributes very little if at all to the observational deficit. Therefore, this study focuses on the heat extracted by ventilated circulation.

A recent analysis of oceanic heat flow measurements suggests that the observed heat flow deficit (difference between the predicted and observed) is reduced by restricting observations to regions with thick sediment cover. Conversely, restricting observations to regions with thin sediment cover increases the observational deficit (Fig. 1A and B, and Hasterok et al., 2011). The differences in the observational deficit and associated area of these thin and thick sediment cover regions affects the total power deficit (integrated heat flow deficit with respect to area).

Recent modeling of the seafloor age distributions (Müller et al., 2008), a new update to the global heat flow database (Hasterok, 2010), and a new plate cooling model calibrated using heat flow (Hasterok, 2013) provide the motivation for a fresh examination of the global power deficit. Beyond updating datasets, incorporating more appropriate statistical estimates of the uncertainty, we investigate the magnitude and spatial extent of ventilated hydrothermal circulation in relation to sediment thickness.

2. Model inputs

The total power deficit can be estimated using heat flow observations by (Wolery and Sleep, 1976)

E-mail address: dhasterok@gmail.com.
[1] Now at University of Adelaide, North Terrace, SA, 5005, Australia.

0012-821X/$ – see front matter
http://dx.doi.org/10.1016/j.epsl.2013.08.016

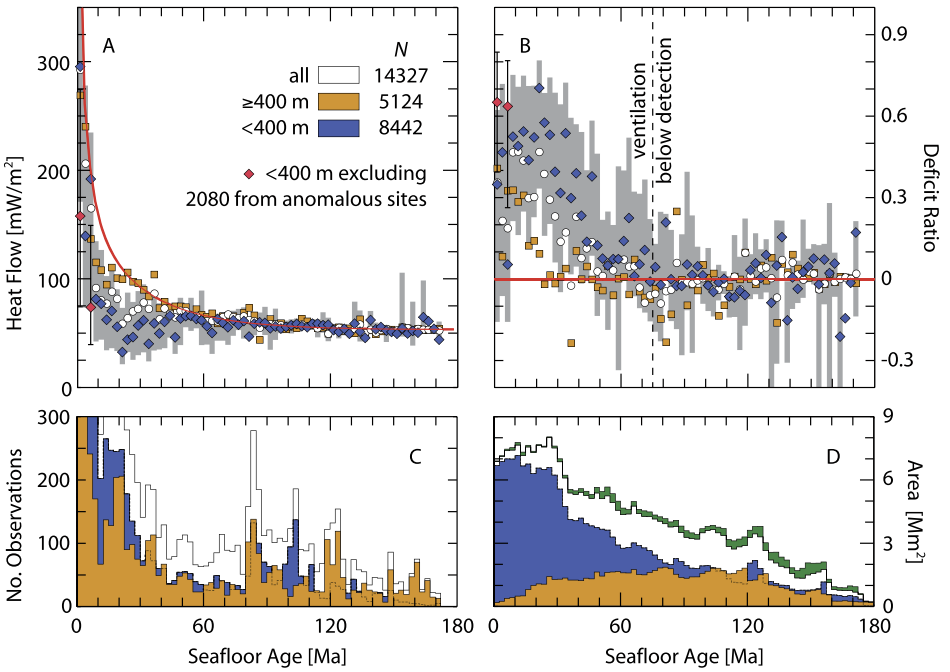

Fig. 1. A summary of oceanic heat flow and seafloor area. (A) Median unfiltered (white circles), filtered for locations with <400 m of sediment cover (blue diamonds), and for locations with ⩾400 m of sediment cover (orange squares) heat flow as a function of seafloor age in 2.5 m.y. bins. Conductive heat flow (red line) is estimated from the plate model by Hasterok (2013). Interquartile range for heat flow with <400 m of sediment cover shown in grey. Red diamonds exclude 2060 measurements from high-resolution surveys with thick sedimentary cover. Data from large igneous provinces (LIPs) are excluded from this analysis. (B) The deficit ratio is defined as 1 − the ratio of observed to conductive heat flow. Symbols are the same as in (A). Dashed line at 75 Ma represents maximum extent of significant ventilated hydrothermal circulation. (C) Number of heat flow determinations within each bin from (A) which colors corresponding to the symbols in (A). Dashed line represents top of obscured histogram. (D) Histograms of seafloor area (Müller et al., 2008) supplemented with age data for the Red Sea. Colors corresponding to datasets in (A). Green field represents the addition of LIPs to the total seafloor area (green). Areas are reported in Mm^2 (10^{12} m^2). Binned heat flow and area are provided as a supplementary material. (For interpretation of the references to color in this figure legend, the reader is referred to the web version of this article.)

$$P = \sum_{i=1}^{N} (\hat{q}_i - q_i) A_i, \tag{1}$$

where $\hat{q}_i$ and q_i are the predicted and observed heat flow between isochrons t_i and t_{i-1} with associated area, A_i. Previous estimates of the global power deficit suggest 27 to 40% of the heat lost through the oceanic crust is redistributed by hydrothermal circulation (Stein and Stein, 1992; Davies and Davies, 2010). We revisit these previous estimates as new datasets for heat flow and age and a new conductive cooling model are now available.

2.1. Heat flow, q

2.1.1. Updated heat flow database

Previous studies used substantially fewer heat flow measurements, 3347 (Sclater et al., 1980) and 5539 (Stein and Stein, 1992), than used in this study. Starting with 14 327 oceanic heat flow measurements (Fig. 2) from an updated global heat flow database (Hasterok, 2010), we are now able to more rigorously estimate the heat flow deficit and areal extent of ventilated hydrothermal circulation. The heat flow observations are corrected for sedimentation using the method of Von Herzen and Uyeda (1963) as detailed by Hasterok et al. (2011). In general, the data coverage is sparse but well distributed geographically over most of the oceans; however, the Southern Ocean, Arctic Ocean, and Pacific Ocean south of ∼30°S have relatively few measurements. Large igneous provinces (LIPs) are shown to exhibit very little heat flow deficit (Hasterok, 2013) and are excluded from this analysis.

The observed (unfiltered) heat flow data exhibit a significant heat flow deficit relative to the conductive cooling model (Fig. 1). The deficit is greatest on young seafloor with the deficit ratio ($1 - q_i/\hat{q}_i$) approaching 0.5 (Fig. 1B). The deficit in observed heat flow values extends to a maximum age between 45 and 65 Ma seafloor.

2.1.2. Filtering heat flow

Oceanic sediments are several orders of magnitude less permeable than the igneous basement below (Spinelli et al., 2004). As a result sediments act as an impermeable barrier to the flow of hydrothermal fluids between the ocean and crust. Flow continues through the subsurface between basement outcrops, with fluid transport 20 to 40 km in some instances, and extracts heat along the entire flow path (Davis et al., 1999; Hutnak et al., 2008). Once the sediment cover blankets all outcrops the ventilated flow ceases, requiring conduction to transport heat to the surface.

A recent study (Hasterok et al., 2011) showed that by globally restricting heat flow observations to sites with a minimum sediment thickness of 400 m and minimum distance to seamounts of 60 km, the background conductive heat loss can be largely recovered (Fig. 1A and B). To determine the appropriate sediment thickness to filter the global dataset, the authors examined the increase in correlation between the restricted data and the half-space cooling model as well as the decrease in variability in binned observations. The estimated sediment thickness filter was determined to be 400 m, but the choice was somewhat arbitrary resulting from relatively uniform high correlation coefficients for sediment thicknesses >350 m (Hasterok et al., 2011). The validity of the 400 m transition is addressed further in Section 4.2. A heat flow deficit persists in regions of thick sediment cover for seafloor ages <25 Ma, although, the associated area is relatively small (Fig. 1B). Stein and Stein (1994) noted the reduction in ventilated circulation in regions of thick sediment, but did not factor it into their total power deficit calculation due to the statistical uncertainty in the projected cutoff age.

Where possible, we use reported sediment thickness values. However, sediment thickness is typically not reported with heat flow observations. In these cases, we use an interpolated digital sediment map (Laske and Masters, 1997; Divins, 2007) to estimate

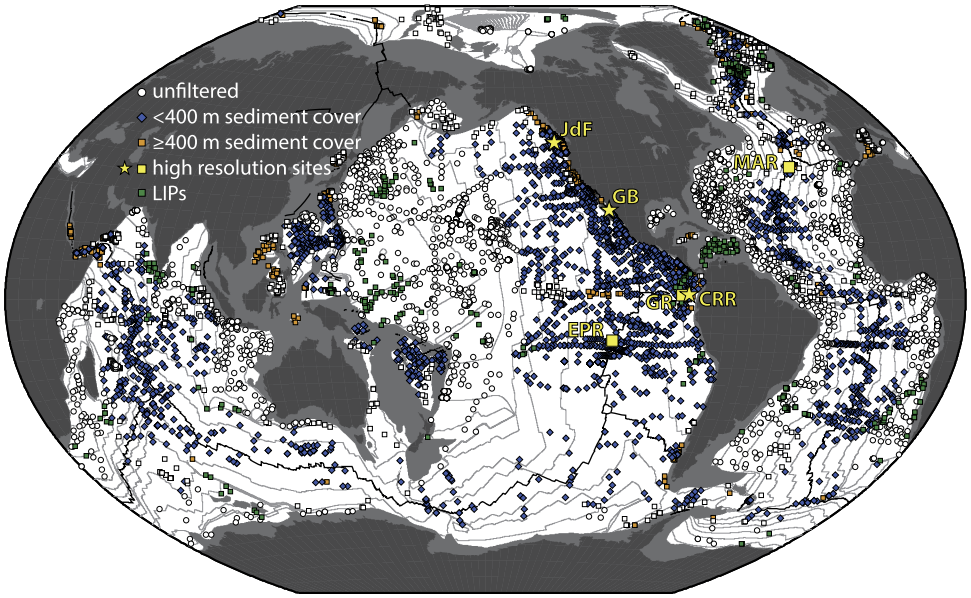

Fig. 2. Oceanic heat flow determination locations. Symbols are defined by age and sediment thickness constraints: orange squares, <25 Ma and ⩾400 m; white squares, 25 Ma to 75 Ma and ⩾400 m; blue diamonds, <75 Ma and <400 m; white circles, ⩾75 Ma and ⩾0 m; and green squares, large igneous provinces. The large yellow squares and stars refer to high-resolution surveys discussed in the text. Abbreviations: JdF, Juan de Fuca rift; GB, Guaymas Basin; CRR, Costa Rica Rift; MAR, Mid-Atlantic Ridge; EPR, East Pacific Rise; and GR, Galapagos Ridge. Age contours in 25 Ma intervals with mid-ocean ridges in bold (Müller et al., 2008). The updated global heat flow database may be found at http://www.heatflow.und.edu/index2.html.

sediment cover at heat flow sites. A concern using such low resolution sediment thickness estimates is that this will result in poor estimates of the true sediment cover. A comparison of sedimentation corrections reported in the literature from direct observation with corrections made using these coarse maps are in reasonable agreement (a majority <15% difference), although, corrections of individual measurements may differ by 40% or more (Fig. 3 of Hasterok et al., 2011). Hence, these coarse maps appear suitable for a global analysis, but likely increase the uncertainty in the estimated deficit.

To estimate the heat flow affected by ventilated circulation we examine the data with 0 to 400 m of sediment cover. These filtered data exhibit lower heat flow relative to the full dataset for ages less than ∼85 Ma and an increase in the deficit ratio >0.1 on average (Fig. 1A and B). At ages >85 Ma there is no systematic difference between the data filtered by sediment thickness, the full dataset, and the conductive cooling model, suggesting ventilated circulation is below a detectable level. Furthermore, the heat flow data do not show a significant deficit ratio at ages older than ∼75 Ma consistent with observations by Stein and Stein (1994). Since the observed heat flow deficit varies by sediment thickness, seafloor area must be restricted in combination with heat flow to accurately estimate the power deficit due to ventilated hydrothermal circulation. Limiting these two quantities results in partially offsetting effects on the total deficit.

2.1.3. *Influence of high-resolution surveys*

High-resolution studies are defined as surveys in which the spatial sampling is close enough such that heat flow anomalies are not aliased and possess sufficient areal coverage that the average can be well characterized. There are quite a few closely sampled profiles within the database. These profiles are, in general, insufficient to accurately characterize the average and contain too few observations within a given age bin to significantly bias the median heat flow.

Three age bins <85 Ma increase in heat flow when filtered by sediment thickness <400 m (Fig. 1A). Two of these age bins, 0 to 2.5 and 5 to 7.5 Ma, exhibit clearly anomalous deficit ratios relative to similar aged lithosphere (Fig. 1B). Close examination of these age bins suggest that the 0 to 2.5 and 5 to 7.5 Ma age bins are biased by high-resolution heat flow surveys that represent a significant fraction of these bin observations (Fig. 3). The third bin with an increase in heat flow (65 to 67.5 Ma) likely results from an insufficient number of observations to accurately characterize the true average and variability.

There are five high-resolution surveys on 0 to 2.5 Ma seafloor. Two of these surveys, located on the Juan de Fuca spreading center and within the Guaymas Basin, are in regions with thick extensive sediment cover (Fig. 3A). Heat flow distributions from these surveys peak just below the plate cooling estimate for 2.5 Ma seafloor with long tails extending to very high values of heat flow (>1000 mW/m^2). Removing observations from these surveys results in a distribution highly skewed to low values—far below conductive estimates—with a near-linear decrease in the frequency of observations between 0 to 500 mW/m^2 (red curve, identified as X in Fig. 3A). A similar heat flow distribution arises in the 5 to 7.5 Ma bin after removal of a high-resolution surveys on the thickly sedimented Costa Rica rift flank (Fig. 3C).

The remaining three high-resolution surveys in the 0 to 2.5 Ma bin have thin sedimentary cover. The stacked heat flow distribution from these three surveys is similar to the distribution without them (Y in Fig. 3B), adding confidence that geographically sparse data can provide a reasonable estimate of the hydrothermal deficit within any given age bin.

Only sites with thick extensive sediment cover strongly bias the estimated heat flow distribution and need to be removed from the dataset prior to estimating the total power deficit. Removing these surveys reduces the total number of data used to estimate the heat flow deficit by 2080. These adjusted heat flow estimates are significantly lower and consistent with the trend in deficit ratio (Fig. 1B red diamonds).

2.2. *Conductive reference model, $\hat{q}$*

Plate cooling models have long been the preferred physically based conductive cooling model used to describe subsidence of

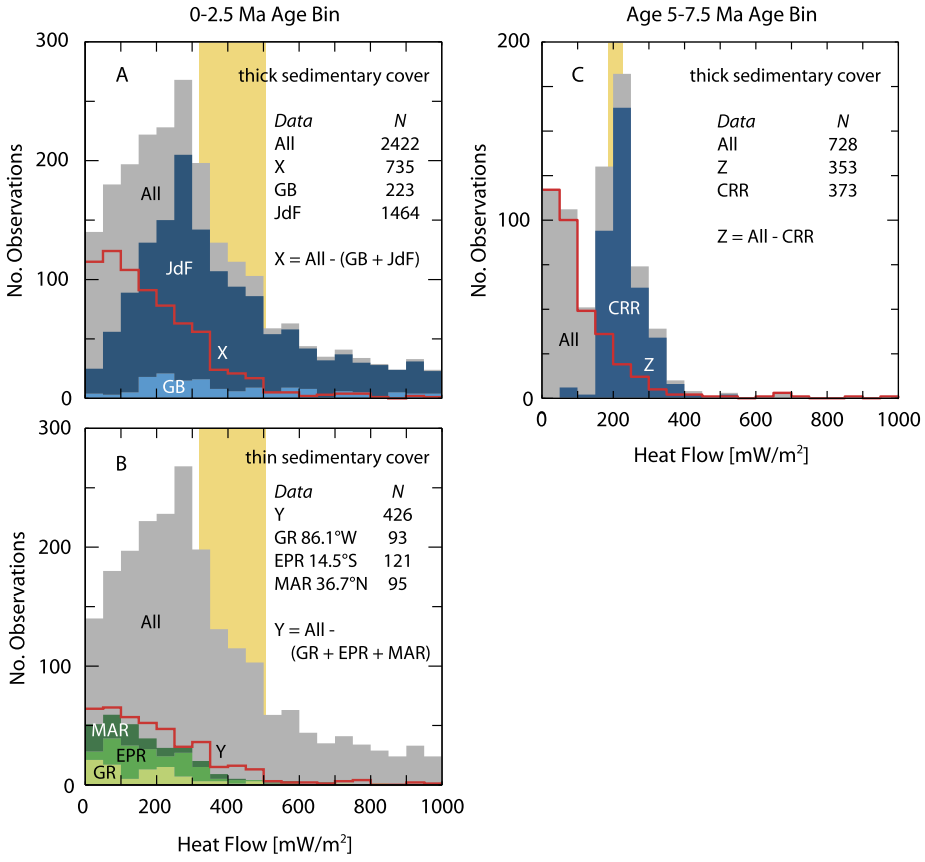

Fig. 3. Heat flow from high-resolution surveys. Analysis of heat flow in 0 to 2.5 Ma (A) and (B) and 5 to 7.5 Ma (C) age bins, respectively. (A) Stacked histograms from high-resolution surveys conducted in regions with thick extensive sediment cover (light blue – GB, Guaymas Basin; dark blue – JdF, Juan de Fuca rift). All data within age bin (grey); all data excluding JdF and GB (red). Estimated conductive heat loss from plate model Hasterok (2013) for 1 to 2.5 Ma (yellow bar). (B) Stacked histograms from high-resolution surveys conducted in regions with thin sediment cover (light green – GR, Galapagos Ridge; medium green – EPR, East Pacific Rise; dark green – MAR, Mid-Atlantic Ridge). All data within age bin (grey); all data excluding high-resolution surveys from (A) and (B) (red). (C) All data within age bin (grey); high-resolution survey from the Costa Rica Rift, CRR (dark blue); and all data excluding CRR (red). (For interpretation of the references to color in this figure legend, the reader is referred to the web version of this article.)

the oceanic lithosphere as it ages (McKenzie, 1967; Parsons and Sclater, 1977; Stein and Stein, 1992; McKenzie et al., 2005; Afonso et al., 2008). The use of heat flow to calibrate plate cooling models has been limited to old seafloor where the effects of hydrothermal circulation are minimal. By restricting heat flow to regions with thick sediment ($\geqslant 400$ m), Hasterok et al. (2011) removed most, if not all, of the hydrothermal deficit on seafloor older than ~25 Ma. The authors supplemented heat flow estimates on seafloor <25 Ma using high-resolution heat flow surveys in regions with thick and extensive sediment cover. Combining these two datasets, it is now possible to calibrate plate cooling models to heat flow observations including the data at young ages (Grose, 2012; Hasterok, 2013).

We use the new model by (Hasterok, 2013) because it fits the observed data well, is calibrated to sediment corrected heat flow, and includes an easy to implement empirical approximation. This cooling model provides a better fit to heat flow data and higher heat flow than GDH1 (Stein and Stein, 1992) on older seafloor, but it is slightly cooler on young seafloor where the observed deficit is greatest.

The empirical approximation for heat flow determined by Hasterok (2013) is

$$\hat{q}(t) = \begin{cases} 506.7t^{-1/2} & \text{if } t \leqslant 48.1, \\ 53 + 106\exp(-0.034607\,t) & \text{if } t > 48.1, \end{cases} \quad (2)$$

where t is time in m.y.

2.3. Seafloor area, A

The area is computed using a digital seafloor age model by Müller et al. (2008), with ages in the Red Sea supplemented using magnetic calibrated dates (Cochran, 1983). Seafloor areas are relatively constant for the first 15 Ma and then begin to fall off nearly linearly to ages of 180 Ma (Fig. 1D). The Müller et al. (2008) seafloor age model is less than the Sclater et al. (1980) model except for a few age bins including the 9 to 20 and 20 to 35 Ma where it is slightly larger. However, the cumulative seafloor area by age is always greater in the Sclater et al. (1980) model. This difference is increased as we ignore the area covered by LIPs for this study. Using this new age model, we expect it to decrease the power deficit relative to previous studies.

3. Model uncertainties

Previous studies assumed Gaussian statistics to estimate uncertainty in the global power deficit (Sclater et al., 1980; Stein and Stein, 1994); however, the distribution of heat flow within hydrothermally affected environments are non-Gaussian, sometimes to an extreme degree. The distribution of heat flow within any given age bin is highly variable, typically skewed towards low values of heat flow with long tailed distributions extending to very high heat flow (Fig. 3). Additionally, Gaussian uncertainties allow for the possibility of negative heat flow values which are highly unlikely except in situations of unstable (warming) bottom water temperatures and are not generally representative of fluid flow or

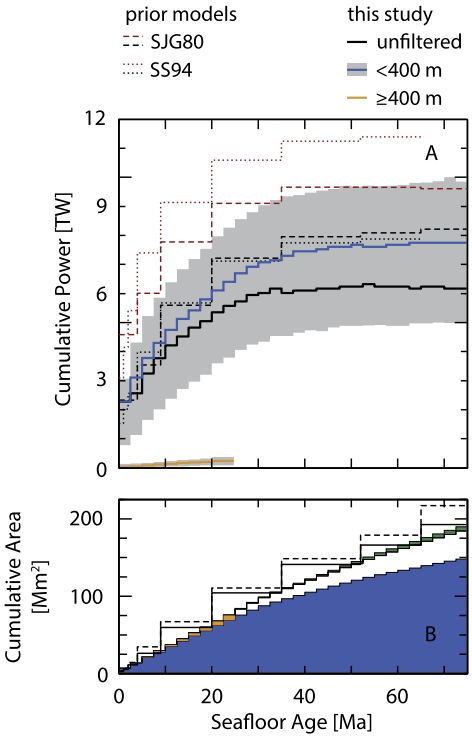

Fig. 4. (A) Cumulative power deficit computed from global heat flow data (unfiltered, bold black) and sediment filtered heat flow data (<400 m, blue; ⩾400 m, orange). Interquartile ranges for sediment filtered estimates in grey. Additional heat flow based models from prior studies: (dashed) SJG80, Sclater et al. (1980); and (dotted) SS94, Stein and Stein (1994). Two curves are shown for the previous studies (dashed/dotted) where the larger in magnitude (red) for each respective study are the original reported value and the smaller in magnitude are recalculated using the same averaging scheme, seafloor age–area model, and plate cooling model. Cumulative power deficit is reported in TW (10^{12} W). (B) Cumulative seafloor area. (dashed line) The area–age model by Sclater et al. (1980) with higher resolution bins 0 to 4 Ma by Stein and Stein (1994). The black line with large bin spacing is the Müller et al. (2008) area–age model calculated with the same bin widths as the dashed line. All other models use Müller et al. (2008) area–age model with 2.5 m.y. bin width. (Blue field) Area–age in regions with <400 m of sediment cover. (Orange field) Area-age in regions with ⩾400 m of sediment cover with ages <25 Ma. (White field) Area–age in regions with ⩾400 m of sediment cover with ages ⩾25 Ma. (Green field) Area–age on LIPs. (For interpretation of the references to color in this figure legend, the reader is referred to the web version of this article.)

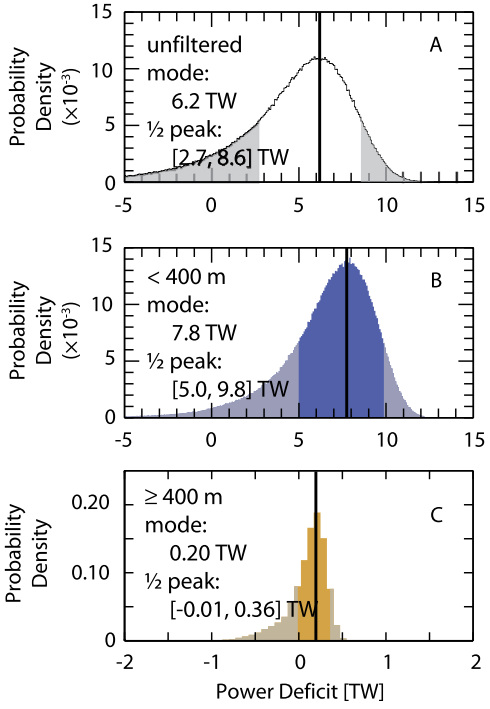

Fig. 5. Oceanic power deficit determined by Monte Carlo analysis using (A) unfiltered heat flow distributions between 0 and 65 Ma, (B) regions with sediment cover <400 m between 0 and 75 Ma, and (C) regions with sediment cover ⩾400 m between 0 and 25 Ma. Half-peak bounds in grey. All models exclude large igneous provinces and high-resolution heat flow surveys with thick extensive sediment cover.

deeper thermal processes. By assuming Gaussian statistics, previous studies bias their average heat flow to values that are too high and possibly place too large an uncertainty on the distribution. As a result, previous estimates of the total power deficit are lower than otherwise expected.

To arrive at a better estimate of the uncertainty we use a Monte Carlo analysis sampling the empirical distribution functions within each age bin derived directly from the heat flow observations. To derive the empirical distribution functions, we divide each age bin into a histogram of heat flow with bin width, δq_i, estimated by $\delta q_i = \sigma_{q_i}/N_i$, where N_i is the number of data within the age interval and σ_{q_i} is the standard deviation of the data subset. A minimum bound of 5 mW/m^2 is imposed for δq_i. Each distribution is randomly sampled 10^6 times using rejection sampling (Ross, 1987, p. 443). The randomly generated set of heat flow deficits are then used to estimate the total power deficit via Eq. (1).

4. Results and discussion

4.1. Unfiltered deficit

Using the unfiltered global data set (full dataset excluding LIPs and high-resolution studies discussed in Section 2.1.3), we derive an estimate of the power deficit (Figs. 4 and 5A). The cumulative power deficit exhibits an increase to ~35 Ma (Fig. 4), increasing only slightly until the deficit ratio reaches zero at ~65 Ma (Fig. 1B).

The total power deficit using the unfiltered heat flow and area at 65 Ma is 6.2 TW. Had the high-resolution surveys been included, the unfiltered estimate would be lower by an additional 1.0 TW with a larger uncertainty (Table 1). The resulting probability distribution function is not Gaussian, but skewed towards low deficit estimates (Fig. 5A). This observation is unsurprising given the long-tailed heat flow distributions within each age interval. Half of the realizations fall between 2.7 and 8.6 TW, giving us a reasonable estimate of the uncertainty.

The unfiltered result will be a useful reference as we examine the influence of sediment filtering on the heat flow and seafloor area used to estimate the total power deficit.

4.2. Filtered deficits

Since the heat flow deficit decreases as sediment cover increases, it would be ideal to estimate the heat flow deficit at several discrete intervals of sediment cover. However, the scatter in the data are too high and the number of observations too poorly distributed in sediment thickness within individual age bins to allow us to do a reliable comprehensive analysis. Therefore, we make a single division between regions with thin and thick sediment cover.

To determine the appropriate sediment cutoff, we perform a series of deficit analyses by examining a subset of the heat flow data with sediment cover between 0 m and a varied maximum value (Fig. 6A). The high-resolution data discussed in Section 2.1.3 are excluded from these tests. The estimated power deficit increases as the maximum sediment cover increases up to 400 m with a heat loss of 7.8 TW. This increase largely mimics the increase in

Table 1
Estimates of thermal power redistributed by hydrothermal circulation in young seafloor.

Reference	Constraint	Age range (Ma)	Power (TW)[a]
Sclater et al. (1980)	heat flow	0–52	8.2[b] (10.1)
Stein and Stein (1994)	heat flow	0–65	7.9[b] (11.3 ± 3.5)
Elderfield and Schultz (1996)	heat flow	1–65	8.8 ± 2
Mottl (2003)	geophysical	0–65	9.9
Spinelli and Harris (2011)	fluid flow	0–65	9
This study (unfiltered)	heat flow	0–67.5	6.2 [2.7, 8.6]
This study (unfiltered)[c]	heat flow	0–67.5	5.2 [1.3, 7.9]
This study (sed. thick <400 m)	heat flow	0–75	7.8 [5.0, 9.8]
This study (sed. thick ⩾400)	heat flow	0–25	0.20 [-0.01, 0.36]

[a] Values in '[]' are uncertainty bounds estimated from half-maximum likelihood probability (Fig. 5).
[b] Power estimates adjusted to common seafloor area model (Müller et al., 2008) and recalculated using plate cooling model by Hasterok (Hasterok, 2013). Values in '()' were previously published estimates.
[c] Includes data from high-resolution surveys with thick sediment cover (JdF, GB, and CCR; see Fig. 3 for abbreviations).

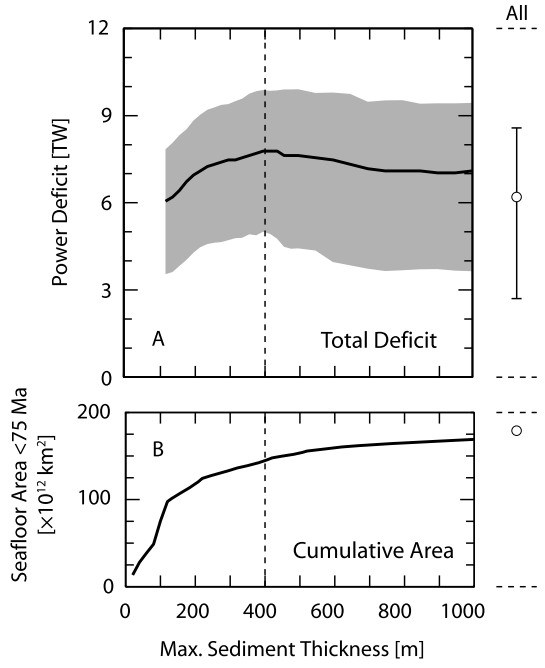

Fig. 6. Effect of sediment filter on hydrothermal estimate. (A) Maximum likely power deficit estimated as a function of maximum sediment bound used to filter heat flow sites. Half-peak uncertainty in grey. Unfiltered estimate (circle) to the right of the plot. Note that all of these exclude the high-resolution surveys in regions with extensive sediment cover. (B) Cumulative seafloor area. Total seafloor area shown to right of plot (circle). Dashed lines represent optimal filter with a maximum sediment thickness <400 m.

cumulative seafloor area (Fig. 6). With sediment cutoffs >400 m the power deficit begins to decrease due to a decrease in the observed heat flow deficit despite an increase in seafloor area.

The optimum choice for sediment filtering is a 400 m cutoff, which is consistent with the preferred filter estimated by Hasterok (2013), though somewhat higher than the transition between advectively- and un-affected heat flow observed by Anderson and Hobart (1976) (150 to 200 m). The higher value observed here likely results from the of global sediment thickness models instead of direct observation. To illustrate why this may be the case, consider a single pixel from the global model which covers an area ~86 km^2 at the equator. It is reasonable to assume that within an area of this size, the sediment thickness can vary considerably, so much so that basement exposures may persist. However, the thicker the sediment cover the fewer, greater distance between, and/or less likely these exposures are to occur. For pixels with 200 m thick cover, basement exposures may be common enough that fluid flow may still impact heat flow observations. Thus, in order to observe the transition between advectively- and un-affected heat flow, a thicker cutoff is required when using global sediment models.

The power deficit determined by limiting heat flow observations to locations with <400 m of sediment cover is ~20% greater than the unfiltered dataset (Table 1, Figs. 6A and 5). The bounds for the full width half-maximum determined using the preferred filter is 5.0 and 9.8 TW, approximately 1 TW narrower bounds than the unfiltered estimate. Therefore, it is necessary to incorporate the effect of sediment when estimating the total power deficit. Additionally, as suggested by the deficit ratio observed in the <400 m filtered data (Fig. 1B), the cumulative power deficit increases to a maximum at 75 Ma, although the increase in the deficit from 50 to 75 Ma is very small <0.2 TW (Fig. 4*A*).

As mentioned previously, a small deficit remains in heat flow data with sediment thicknesses ⩾400 m (Fig. 1A and B). These regions with thick sediment experience half the heat flow deficit for one-third of the duration (25 Ma) of regions with thin sediment cover. The decrease in heat flow deficit when filtering by sediment thickness was previously observed by (Stein and Stein, 1994), but not with a corresponding decrease in heat flow deficit.

To estimate the total power deficit, we must add the small deficit from heat flow data with sediment thicknesses ⩾400 m. This additional power loss due to ventilated circulation is 0.20 TW (Fig. 6B), bringing the best estimate for the total power deficit to 8.0 TW (29% of the oceanic power loss Hasterok, 2013, 17 to 18% of the Earth's total power loss, Pollack et al., 1993; Jaupart et al., 2007; Davies and Davies, 2010).

4.3. Sensitivity tests

The reference dataset used for all sensitivity tests (unless otherwise noted) is filtered for locations with <400 m sediment thickness and excludes high-resolution studies as discussed in Section 2.1.3.

4.3.1. Averaging scheme and bin width

The effect of the averaging scheme makes a relatively large difference in the estimated power deficit. This study uses a median value of the reference conductive cooling curve whereas previous studies used the mean value within each age bin (Sclater et al., 1980; Stein and Stein, 1994). Because the cooling curve is convex down, the mean value is larger than the median. For example within the first seafloor age bin (0 to 2.5 Ma), the function mean is 641 mW/m^2 whereas the median is 453 mW/m^2. The difference in averaging schemes is a significant fraction of the total power estimate, 1.3 TW, when using median rather than mean values (Table 2).

To determine which averaging scheme is appropriate, we compute the total power deficit using several bin widths between 1.5

Table 2
Sensitivity of model construct/inputs expressed as a difference from the reference model.[a]

Test	Power difference (TW)
Bin size	0.0
Averaging scheme[b]	−1.3
Gaussian statistics	1.8
Sediment correction	0.4
Plate cooling model[c]	−0.07
Seafloor age–area function[d]	−2.0

[a] The total power deficit model used as a reference for these tests: sediment corrected heat flow in 2.5 m.y. age bins; <400 m of sediment cover; the median values of the plate model by Hasterok (2013); and seafloor area by Müller et al. (2008).
[b] Median versus mean of plate cooling model within bin ages.
[c] Using the plate cooling model by Stein and Stein (1992).
[d] Using seafloor age–area by Sclater et al. (1980).

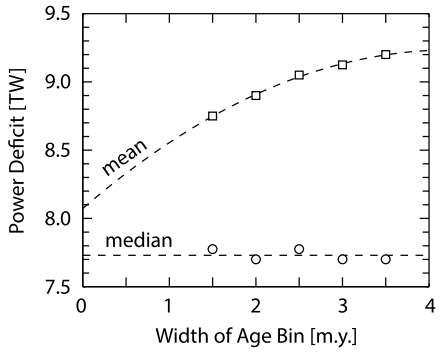

Fig. 7. Effect of averaging scheme and bin width on estimated power deficit. Averaging schemes: mean of cooling model (squares); median of cooling model (circles). Dashed lines represent extrapolations to zero bin width.

and 3.5 Ma (Fig. 7). The estimated total power deficit is nearly independent of the bin size chosen when the median averaging scheme is used. Using the mean averaging scheme, the total power deficit increases with bin size from 8.8 TW at 1.5 m.y. to 9.2 TW at 3.5 m.y. Extrapolating the total power deficits computed using the mean averaging scheme to 0 m.y. bin width via a quadratic fit yields an estimated 8.1 TW, which is much closer to the 7.7 TW estimated via the median averaging scheme. This effect could be anticipated because the average of the cooling function within any given time interval approaches the median value as the bin size decreases. Therefore, using the median rather than mean provides a more reliable estimate of the total power deficit.

While the scatter in median heat flow between bins increases with decreasing bin size, the full-width at half-maximum determined by the Monte Carlo analysis increases linearly by 33% from a bin size of 1.5 to 3.5 m.y. Thus our choice of a bin size, 2.5 m.y., may be a conservative estimate of the uncertainty but does not bias the total estimated deficit.

4.3.2. Sedimentation correction

The sediment correction increases the median heat flow by 10% or less for regions with thick sediment (Hasterok et al., 2011), and the correction is smaller still in regions with thin sediment. Additionally, the plate cooling model we use is calibrated using sediment corrected heat flow with thick sediment cover which results in a higher predicted heat flow. Therefore, we expect the net effect of the sediment correction to increase the power deficit slightly relative to uncorrected heat flow data.

In order to determine the effect of the sediment correction we need a plate model calibrated using uncorrected heat flow data. We follow the method of Hasterok (2013) to derive an uncorrected plate model

$$\hat{q}(t) = \begin{cases} 494.9t^{-1/2} & \text{if } t \leqslant 49.3, \\ 49.1 + 98.2\exp(-0.030970t) & \text{if } t > 49.3. \end{cases} \quad (3)$$

Using the uncorrected heat flow data and the uncorrected reference heat flow defined above, the power deficit for region with <400 m of sediment cover is 7.4 TW. Thus, including the sediment correction increases the estimated power deficit by 0.4 TW or ∼5% (Table 2). The effect on the full-width at half-maximum is minimal.

4.3.3. Reference cooling model

While there are some differences between the new conductive cooling model (Hasterok, 2013) compared with the previous reference model (Stein and Stein, 1992). Most of the differences between the models occur on old lithosphere. The use of Hasterok (2013) reduces the total power deficit by 0.07 TW due to slightly lower values of heat flow on young seafloor (Table 2). This reduction is insignificant given the uncertainties in the data.

4.3.4. Seafloor age–area function

The seafloor age–area function used by Sclater et al. (1980) and Stein and Stein (1992) has larger and non-uniform bin sizes than our chosen division of 2.5 m.y. (Fig. 4B). We first recompute our result using the same bin divisions before examining the difference in the age–area functions. Using the Müller et al. (2008) relationship results in a 2.0 TW lower power deficit estimate when compared with the Sclater et al. (1980) model (Table 2).

4.3.5. Gaussian statistics

A great deal of effort in this study is placed on accurately assessing uncertainties in the heat flow distributions and how this translates into uncertainties in the total power deficit. Previous studies assume Gaussian statistics. While we cannot easily test the effect of Gaussian versus non-Gaussian statistics on those datasets, we can test its importance for this dataset.

Using Gaussian statistics we estimate the total power deficit to be 6.0 TW with a standard deviation of 2.9 TW. Hence, the use of Gaussian statistics decreases the estimated total power deficit by 1.8 TW (Table 2).

There is also a significant effect on the bounds. Because the distributions estimated using non-Gaussian distributions are skewed, we use the half-maximum probabilities to estimate the bounds. The bounds estimated at the half-maximum for the Gaussian statistics is 2.7 and 9.4 TW, respectively. The lower bound is 117% larger and the upper bound 170% larger when Gaussian statistics are used rather than the non-Gaussian distributions. Therefore, the use of Gaussian statistics inflates the bounds of uncertainty, with the greatest effect on the upper bound.

4.4. Comparison with previous studies

The total power deficit estimated from this study (8.0 TW) is less than previous heat flow based estimates by 2 to 3 TW (20 to 30%) and ∼1 TW (11%) less than fluid flow estimates (Table 1). A number of geochemical constraints have also been employed to estimate the power deficit, but they yield a large scatter between methods with widely varying degrees of precision (Elderfield and Schultz, 1996). Hence the geophysical based models likely yield more accurate estimates of heat loss (Mottl, 2003).

The previous models presented in Table 1 are based on averaging entire global datasets, without restricting area by sediment thickness constraints. A direct comparison of the global (unfiltered) dataset used in this study (6.2 TW) to previous estimates results in a greater disparity in the estimated power deficit (4 to 5 TW) (Table 1). To directly compare the results from prior studies, we recalculate prior estimates using the same averaging scheme, age–area function, and plate cooling model (Fig. 4A). After recalculating, estimates from previous studies are closer to our unfiltered

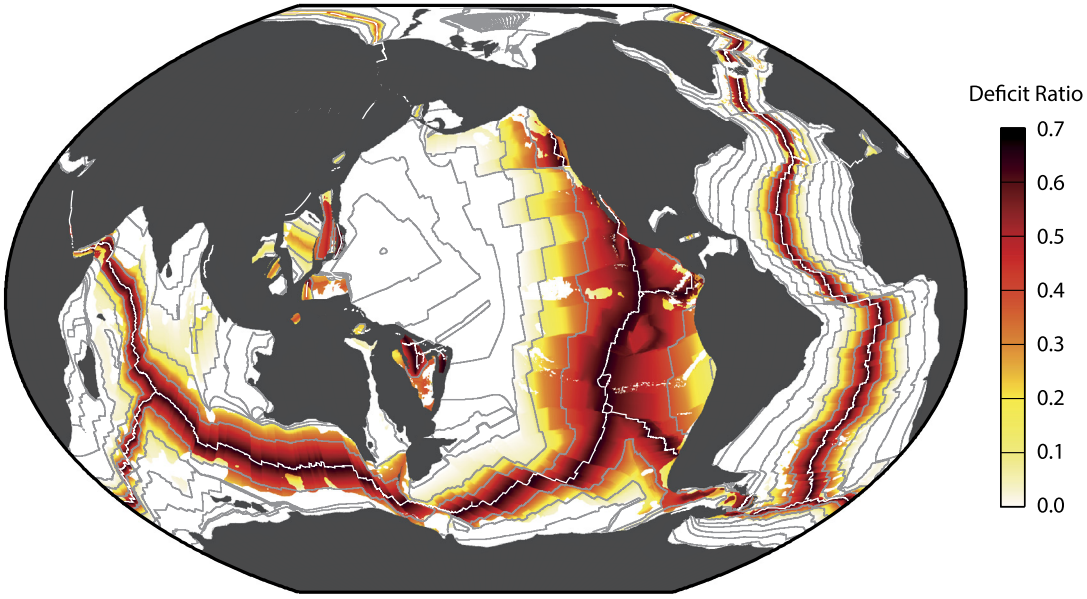

Fig. 8. Inferred regions with heat flow deficit due to ventilated hydrothermal circulation. Deficit ratio estimates from Eqs. (4) and (5).

dataset (Table 1). Approximately 1.9 TW for Sclater et al. (1980) and 3.4 TW for Stein and Stein (1994) can be attributed to these processing/model differences. Some of the remaining difference (1.7 to 2.0 TW) may result from the use of means rather than medians of binned data and larger bin sizes than simply the updated dataset.

Although, the uncertainty bounds on the deficit between this and previous heat flow studies are equivalent given the scatter in the data, the new dataset used in this study incorporates the previous data and really represents a shift in the bounds and maximum likelihood estimate, which is important for modeling studies that use the global power deficit as a constraint.

4.5. Spatial variation in hydrothermal activity

To examine the spatial patterns in the ventilated hydrothermal deficit, it is convenient to obtain an empirical approximation for the deficit ratio. We offer the following empirical relations for the deficit ratio: for regions with sediment cover <400 and seafloor ages <75 Ma,

$$(1-q/\hat{q}) = \begin{cases} 0.66 - 0.0111t & \text{if } t < 55, \\ 0.186 - 0.0025t & \text{if } 55 < t < 75, \end{cases} \tag{4}$$

and for sediment cover $\geqslant 400$ m and seafloor ages <25 Ma,

$$(1-q/\hat{q}) = 0.40 - 0.016t. \tag{5}$$

A simple linear fit to the deficit ratio in Fig. 1B yields power deficit estimates that are much too high so we tailor the approximation to yield a value closer to our modal estimate.

The oceanic lithosphere covers 58% (298 Mm^2) of the Earth's surface but only a fraction of the total area is presently affected by ventilated hydrothermal circulation (Fig. 1C and 8). Using our constraints on the distribution of observed deficit, we estimate 51% of the seafloor area (30% of the Earth's surface) presently experiences ventilated hydrothermal circulation. This estimate includes 144.7 Mm^2 in regions of thin sediment cover (<400 m) to 75 Ma and 6.2 Mm^2 in regions of thick sediment cover ($\geqslant 400$ m) to 25 Ma.

We deduce from the heat flow observations that the entire oceanic crust experiences interaction with hydrothermal fluids during its temporal evolution, although the magnitude varies. From the deficit observations (Fig. 1B), we predict half as much heat transfer by ventilation in regions with thick sediment and for approximately one-third of the duration. While the total area covered by thick sediment is comparatively small, the influence on lithospheric evolution and biological communities could be important locally.

4.6. Future directions

The vigor of hydrothermal circulation in any given locality is dependent upon a number of factors including, but not limited to, the sediment thickness, basement permeability, geometry of igneous exposures, and the heat flow into the base of the advecting layer. However, this is intractable on a global scale as the datasets necessary to determine/estimate these parameters do not exist in all instances. Although the sediment thickness, for which global models do exist, may also serve as a proxy for the likelihood of basement exposures as it stands to reason that as sediment thickens it covers a spatially larger area in addition to an increase in the vertical dimension. Basal heat flow is largely controlled by the conductive cooling of the lithosphere and therefore implicit in the estimated lithospheric cooling curve. The permeability of the basement is far more difficult to estimate and leads to scatter in the heat flow observations globally and can be viewed as a contribution to the uncertainty.

A provocative recent study by Spinelli and Harris (2011) examined the influence of legacy effects on the cumulative heat loss by ventilated circulation. The legacy effects give rise to an underprediction in the total heat extracted near the ridge and overprediction on the flanks whereas the total heat extracted may be correct. While their estimated power deficit is similar to ours (Table 1), they test only one possible set of model parameters based on estimates from direct observation at a few localities. However, one could use the power deficit and its probability density as a constraint on the uncertainties/variability of physical inputs to numerical models of ventilated flow.

5. Conclusions

Understanding the processes controlling the distribution and magnitude of hydrothermal fluid flow are important for understanding the physical and chemical evolution of the ocean and

lithosphere. This study provides a global estimate of the spatial distribution and magnitude of ventilated hydrothermal deficit in heat flow. To further improve the global estimate it is important to take into consideration more regional variations in lithospheric cooling, improve the resolution and accuracy of sediment cover and sedimentation history, and increase the number of heat flow data to better characterize the regional hydrothermal systems as well as fill significant gaps in coverage, particularly in the southern and Arctic oceans.

We estimate total power deficit associated with ventilated hydrothermal circulation to be 8.0 TW with a full-width at half-maximum of 5 TW. This deficit represents 29% of heat loss through the oceanic lithosphere and 17 to 18% of the total global heat loss.

Our best estimate of the total power deficit represents a downward revision of 2 to 3 TW compared with previous heat flow based studies. This downward revision is a result of differences (in order of importance) in non-Gaussian versus Gaussian statistics, the seafloor area–age model, sediment filtering, the averaging scheme, the heat flow dataset, and the plate cooling model.

The majority, 7.8 TW, is due to vigorous circulation in regions of thin sediment cover ($<$400 m) with the remaining 0.2 TW in regions of thick sediment cover ($\geqslant$400 m). The effects of ventilated hydrothermal circulation extend to 75 Ma in regions with thin sediment and to 25 Ma in regions with thick sediment. We estimate 51% of the present day seafloor area is affected by ventilated hydrothermal circulation.

This improved estimate may serve as a rigorous constraint for future modeling studies of ventilated hydrothermal circulation on a global scale.

Acknowledgements

Funding for D.H. was provided by the Green Foundation at UCSD-IGPP. D.H. thanks D.S. Chapman, J. Sclater, and L.A. Coogan, for helpful discussions and comments on earlier versions of the manuscript. D.H. also thanks two anonymous reviewers.

Appendix A. Supplementary material

Supplementary material related to this article can be found online at http://dx.doi.org/10.1016/j.epsl.2013.08.016.

References

Afonso, J., Fernàndez, M., Ranalli, G., Griffin, W., Connolly, J., 2008. Integrated geophysical–petrological modeling of the lithosphere and sublithospheric upper mantle: Methodology and applications. Geochem. Geophys. Geosyst. 9, Q05008.

Anderson, R., Hobart, M., 1976. The relation between heat flow, sediment thickness, and age in the eastern Pacific. J. Geophys. Res. 81, 2968–2989.

Cochran, J., 1983. A model for the development of the Red Sea. Am. Assoc. Pet. Geol. Bull. 67, 42–69.

Davies, J., Davies, D., 2010. Earth's surface heat flux. Solid Earth 1, 5–24.

Davis, E., Elderfield, H. (Eds.), 2004. Hydrology of the Oceanic Lithosphere. Cambridge University Press, London.

Davis, E., Lister, C., 1977. Heat flow measured over the Juan de Fuca ridge: evidence for wide spread hydrothermal circulation in a highly heat transportive crust. J. Geophys. Res. 82, 4845–4860.

Davis, E., Chapman, D., Wang, K., Villinger, H., Fisher, A., Robinson, S., Grigel, J., Pribnow, D., Stein, J., Becker, K., 1999. Regional heat flow variations across the sedimented Juan de Fuca Ridge eastern flank: constraints on lithospheric cooling and lateral hydrothermal heat transport. J. Geophys. Res. 104, 17675–17688.

Divins, D., 2007. Total sediment thickness of the world's oceans & marginal seas. Tech. rep., NGDC, NOAA, http://www.ngdc.noaa.gov/mgg/sedthick/sedthick.html.

Elderfield, H., Schultz, A., 1996. Mid-ocean ridge hydrothermal flux and the chemical composition of the ocean. Annu. Rev. Earth Planet. Sci. 24, 191–224.

Fisher, A., Von Herzen, R., 2005. Models of hydrothermal circulation within 106 Ma seafloor: Constraints on the vigor of fluid circulation and crustal properties, below the Madeira abyssal plain. Geochem. Geophys. Geosyst. 6, Q11001.

Grose, C., 2012. Properties of oceanic lithosphere: revised plate cooling model predictions. Earth Planet. Sci. Lett. 333–334, 250–264.

Hasterok, D., 2010. Thermal state of the oceanic and continental lithosphere. Ph.D. thesis. University of Utah.

Hasterok, D., 2013. A heat flow based cooling model for tectonic plates. Earth Planet. Sci. Lett. 361, 34–43.

Hasterok, D., Chapman, D., Davis, E., 2011. Oceanic heat flow: Implications for global heat loss. Earth Planet. Sci. Lett. 311, 386–395.

Hutnak, M., Fisher, A., Harris, R., Stein, C., Wang, K., Spinelli, G., Schindler, M., Villinger, H., Silver, E., 2008. Large heat and fluid flux driven through mid-plate outcrops on ocean crust. Nat. Geosci. 1, 611–614.

Jaupart, C., Labrosse, S., Mareschal, J.-C., 2007. Temperatures, heat and energy in the mantle of the Earth. In: Shubert, G., Bercovici, D. (Eds.), Treatise on Geophysics: Mantle Dynamics, vol. 7. Elsevier, pp. 253–303. Ch. 6.

Laske, G., Masters, G., 1997. A global digital map of sediment thickness. EOS Trans. AGU 78, F483.

Lister, C., 1972. On the thermal balance of a mid-ocean ridge. Geophys. J. R. Astron. Soc. 26, 515–535.

McKenzie, D., 1967. Some remarks on heat flow and gravity anomalies. J. Geophys. Res. 72, 6261–6273.

McKenzie, D., Jackson, J., Priestley, K., 2005. Thermal structure of oceanic and continental lithosphere. Earth Planet. Sci. Lett. 233, 337–349.

Mottl, M., 2003. Partitioning of energy and mass fluxes between midocean ridge axes and flanks at high and low temperature. In: Halbach, P., Tunnicliffe, V., Hein, J. (Eds.), Energy and Mass Transfer in Marine Hydrothermal Systems. Dahlem University Press, pp. 271–286.

Müller, R., Sdrolias, M., Gaina, C., Roest, W., 2008. Age, spreading rates, and spreading asymmetry of the world's ocean crust. Geochem. Geophys. Geosyst. 9, Q04006, http://dx.doi.org/10.1029/2007GC001743.

Parsons, B., Sclater, J., 1977. An analysis of the variation of ocean floor bathymetry and heat flow with age. J. Geophys. Res. 82, 803–827.

Pollack, H., Hurter, S., Johnson, J., 1993. Heat flow from the Earth's interior: analysis of the global data set. Rev. Geophys. 31, 267–280.

Ross, S., 1987. Introduction to Probability and Statistics for Engineers and Scientists. Probab. Math. Stat. Wiley, New York.

Sclater, J., Crowe, J., Anderson, R., 1976. On the reliability of oceanic heat flow averages. J. Geophys. Res. 81, 2997–3006.

Sclater, J., Jaupart, C., Galson, D., 1980. The heat flow through the oceanic and continental crust and the heat loss of the Earth. Rev. Geophys. Space Phys. 18, 269–311.

Spinelli, G., Giambalvo, E., Fisher, A., 2004. Sediment permeability, distribution, and influence on fluxes in oceanic basement. In: Davis, E., Elderfield, H. (Eds.), Hydrology of the Oceanic Lithosphere. Cambridge University Press, London, pp. 151–188.

Spinelli, G., Harris, R., 2011. Legacy of axial cooling affects partitioning of hydrothermal heat extraction from oceanic lithosphere. J. Geophys. Res. 116, B09102.

Stein, C., Stein, S., 1992. A model for the global variation in oceanic depth and heat flow with lithospheric age. Nature 359, 123–129.

Stein, C., Stein, S., 1994. Constraints on hydrothermal flux through the oceanic lithosphere from global heat flow. J. Geophys. Res. 99, 3081–3095.

Von Herzen, R., Uyeda, S., 1963. Heat flow through the eastern Pacific Ocean floor. J. Geophys. Res. 68, 4219–4250.

Williams, D., Von Herzen, R., 1974. Heat loss from the Earth: new estimate. Geology 2, 327–328.

Wolery, T., Sleep, N., 1976. Hydrothermal circulation and geochemical flux at mid-ocean ridges. J. Geol. 84 (3), 249–275.